March 2002 • NREL/SR-520-31739

Subcontractor Report

Thin Film CIGS Photovoltaic Technology

Final Technical Report
16 April 1998 – 15 October 2001

A.E. Delahoy, J. Cambridge, L. Chen,
and Z.J. Kiss
Energy Photovoltaics, Inc.
Princeton, New Jersey

National Renewable Energy Laboratory

1617 Cole Boulevard
Golden, Colorado 80401-3393

NREL is a U.S. Department of Energy Laboratory
Operated by Midwest Research Institute • Battelle • Bechtel

Contract No. DE-AC36-99-GO10337

March 2002 • NREL/SR-520-31739

Thin Film CIGS Photovoltaic Technology

Final Technical Report
16 April 1998 – 15 October 2001

A.E. Delahoy, J. Cambridge, L. Chen,
and Z.J. Kiss
Energy Photovoltaics, Inc.
Princeton, New Jersey

NREL Technical Monitor: Harin S. Ullal

Prepared under Subcontract No. ZAK-8-17619-21

National Renewable Energy Laboratory

1617 Cole Boulevard
Golden, Colorado 80401-3393

NREL is a U.S. Department of Energy Laboratory
Operated by Midwest Research Institute • Battelle • Bechtel

Contract No. DE-AC36-99-GO10337

NOTICE

Available electronically at http://www.osti.gov/bridge

Available for a processing fee to U.S. Department of Energy
and its contractors, in paper, from:

U.S. Department of Energy
Office of Scientific and Technical Information
P.O. Box 62
Oak Ridge, TN 37831-0062
phone: 865.576.8401
fax: 865.576.5728
email: reports@adonis.osti.gov

Available for sale to the public, in paper, from:

U.S. Department of Commerce
National Technical Information Service
5285 Port Royal Road
Springfield, VA 22161
phone: 800.553.6847
fax: 703.605.6900
email: orders@ntis.fedworld.gov
online ordering: http://www.ntis.gov/ordering.htm

Printed on paper containing at least 50% wastepaper, including 20% postconsumer waste

Preface

Energy Photovoltaics, Inc. (EPV) has been engaged in the research and development of thin-film $CuInSe_2$ (CIS) and $Cu(In,Ga)Se_2$ (CIGS) photovoltaic technology since 1991. During its previous 3-year research subcontract that ended in April 1998, EPV demonstrated a 9.7% CIGS minimodule and a 7.6%, 3100 cm^2, unencapsulated CIGS module that produced 24 watts. Prototype a-Si/CIGS tandem modules were also produced. EPV has consistently pursued a vacuum-based approach to CIGS production, using low-cost glass substrates and novel source technology. It has also chosen to develop processing methods with worker safety in mind. It is believed that these choices will pay off in terms of layers with good uniformity and low defects, and production without significant hazards. These features should help reduce the manufacturing cost of CIGS.

Thin film PV technologies have advanced considerably in the last few years. Their reliability and low material costs are enabling them to enter the market in parallel with wafer-based PV [1]. At the time of writing, the leading thin film technologies have exhibited the following record efficiencies and powers for large area modules:

CIGS	12.1%	44.3W	Siemens Solar (CIGSS)
	10.4%	68.9W	Wurth Solar
CdTe	11.0%	92.5W	BP Solar
	11%	59W	Matsushita
	10.1%	67.1W	First Solar
a-Si/x-Si	10%	38W	Kaneka
a-Si triple	7.9%	35.7W	United Solar
a-Si dual	7.6%	56W	BP Solar

It may be noted that CIGSS continues to hold the efficiency record.

EPV's thin film manufacturing prowess may be gauged by examining its production of tandem junction, amorphous silicon PV modules, model EPV-40. The modules are listed by Underwriters Laboratories, Inc. (UL). The main production is by DUNASOLAR in Hungary, using an *Integrated Manufacturing System* that encompasses equipment, process and training supplied by EPV. Additional production is underway at EPV in New Jersey and at CALSOLAR in California.

This three-phase, cost-shared subcontract with NREL is entitled "Thin-Film CIGS Photovoltaic Technology." The subcontract is part of the **NREL Thin-Film Partnership Program**, and EPV participates in the National CIS Team Meetings. One objective of this subcontract (ZAK-8-17619-21) is to demonstrate the required deposition control to produce CIGS modules at a substrate size of 4300 cm^2. The processing also needs to be fast enough to be compatible with high throughput manufacturing. This final technical report mentions highlights of the first and second phases of the subcontract, and describes in detail results obtained during the third phase of the subcontract (April 16, 2000 - August 15, 2001).

CONTENTS

TABLES

FIGURES

1.0 Introduction

As part of the Thin Film Partnership Program, Energy Photovoltaics, Inc. has conducted research to support a technology base for production of CIGS PV modules based on vacuum deposition onto glass. To prepare CIGS on large glass substrates (currently 0.43m^2, with scale up to 0.79m^2 in progress), EPV delivers materials (including Cu) from line sources to a substrate that is translated in a direction perpendicular to the axis of the source.

Concerning the background to this approach, it may be observed that while several methods of forming device quality CIGS have been developed (e.g. vacuum deposition, atmospheric pressure selenization of metallic precursors, rapid thermal processing, or electrodeposition,) vacuum deposition has repeatedly achieved the world record for the highest efficiency CIGS device. Thus, in 1998, a record thin-film solar cell efficiency (18.8% for 0.44 cm^2) was achieved by NREL using vacuum-deposited CIGS [2]. The deposition employs four point sources and flux integration for process control. However, no group in the US has fabricated a large (> 0.1 m^2) and efficient module using the NREL 3-stage process (or any other vacuum process) because of the difficulties facing scale-up and the lack of off-the-shelf evaporative sources suitable for large area coating. To overcome these manufacturing barriers, EPV has developed vacuum equipment incorporating novel linear evaporation sources designed for uniform coating of large substrates [3]. The use of elemental selenium avoids the need for gaseous hydrogen selenide and provides for a safe manufacturing environment.

Project Objective: The overall objective of this R&D program has been to develop processing procedures and recipes and to implement them on novel, large-scale, all-vacuum coating equipment to produce high efficiency, thin film CIGS PV modules. Sub-objectives included: investigation of various CIGS formation methods, linear source characterization, a CIGS process capable of better than 15% device efficiency, transfer of process to a 4300 cm^2 system, demonstrated control of Cu/(In+Ga) and Ga/(In+Ga) ratios, an optimized Mo back electrode, utilization of a Cd-free buffer layer, high rate ZnO deposition, and low loss patterning operations. These goals were chosen to provide a foundation for manufacturing of CIGS modules using safe, all-vacuum processing.

Approach: R&D and process development for CIGS were conducted in the Hercules 4-source system (six 5cm x 10cm stationary substrates per run) and in the Zeus 4-source system (one 4300 cm^2 moving substrate per run). In the latter system, source materials were delivered downwards to the moving glass using custom-built source heads housing four independent linear evaporative sources, the source axes being perpendicular to the direction of glass travel. This approach allowed a wide range of vacuum-based CIGS recipes to be implemented.

For junction formation, EPV relied on CBD CdS on a day-to-day basis, while exploring alternative methods in parallel. Other methods included the use of $ZnIn_2Se_4$ to form the buffer layer. This was pursued within the EPV sub-team of the National CIS R&D Team. For high rate ZnO deposition, EPV employed planar magnetron sputtering using ceramic ZnO targets. Module encapsulation employed glass-glass vacuum lamination using EVA, with processing similar to that of the EPV-40 tandem junction a-Si module.

Improved film and device characterization were realized through establishment of new laboratories containing ICP-AES, SEM/EDS, and computerized QE facilities.

2.0 Highlights from Phases I and II

Minimodules
During Phase I of this subcontract, EPV produced a 34 cm^2, 16-cell CIGS minimodule using its *FORNAX* process with V_{oc} 9.58V, I_{sc} 52.0 mA, FF 69.8%, and efficiency of 10.2%.

Mo back electrode
During Phase II, large area sputtering of Mo films suitable for supporting very high efficiency cell processing was demonstrated. (It had earlier been shown, through side-by-side CIGS depositions onto various Mo substrates, that the Mo can strongly affect cell efficiency.) Using Mo prepared at EPV by proprietary substrate preparation and Mo sputtering from a 56 cm target using a bi-layer process, NREL deposited a 17.1% CIGS cell (no AR coating) [4]. The Mo was produced on EPV's 0.43 m^2 pilot line equipment. The I-V curve is shown in Fig. 2.1. The parameters of this cell are V_{oc} 644 mV, J_{sc} 35.7 mA cm^{-2}, and FF 74.7%. This result demonstrates that high quality Mo can be produced over large areas.

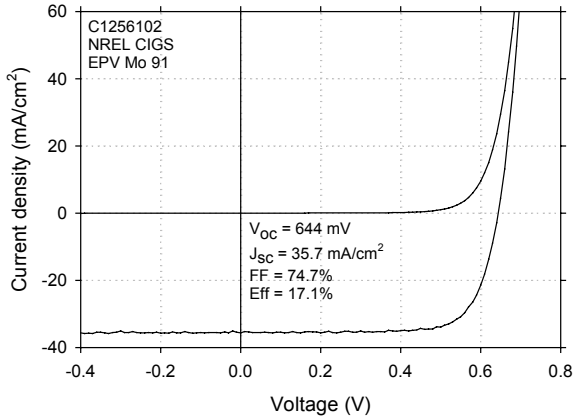

Fig. 2.1. I-V curve of 17.1% cell (NREL CIGS on EPV Mo)

Pilot line CIGS
To monitor the quality of CIGS prepared in the pilot line, small sections of the substrate are processed through the R&D scale CdS/ZnO stations. Figure 2.2 shows the I-V curve of a 12.0% cell with 581 mV V_{oc} prepared using pilot line CIGS [4]. This result demonstrates that high quality CIGS can be prepared by linear source evaporation.

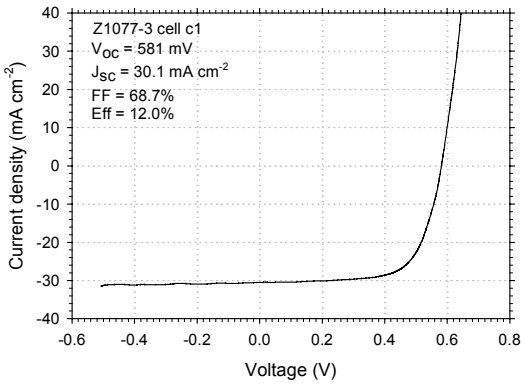

Fig. 2.2. I-V curve for 12.0% cell using pilot line CIGS.

3.0 CIGS Deposition

3.1 R&D Scale

R&D scale CIGS deposition was conducted in the Hercules 4-source system. This system is fitted with open boats for metal deposition and a baffled source for Se. It was recently upgraded to accommodate six 5cm x 10cm stationary substrates per run rather than the four substrates previously accommodated.

3.2 Large Area

Large area CIGS deposition was performed in the Zeus system using linear source evaporation onto moving substrates. Some of EPV's CIGS formation processes were reviewed in [5]. The Zeus system has been shown capable of producing CIGS films of fairly uniform thickness and composition, but further improvement of reproducibility is desirable. A schematic diagram of part of the system is shown below in Fig. 3.1. [6]. As shown in the figure, the glass is transported on rollers, and the equipment is capable of handling glass at the high temperatures necessary to produce high quality CIGS. The system is equipped with four downward-facing linear evaporation sources that may be used for Cu, In, Ga, and Se. To obtain a high source material utilization, the source-substrate distance is relatively short. Of special significance is EPV's ability to build linear sources capable of Cu evaporation. This is a notable technological feat given the high Cu source temperature. CIGS was produced mostly by evaporation of the elements, although compound evaporation and sputtering of Cu were also explored.

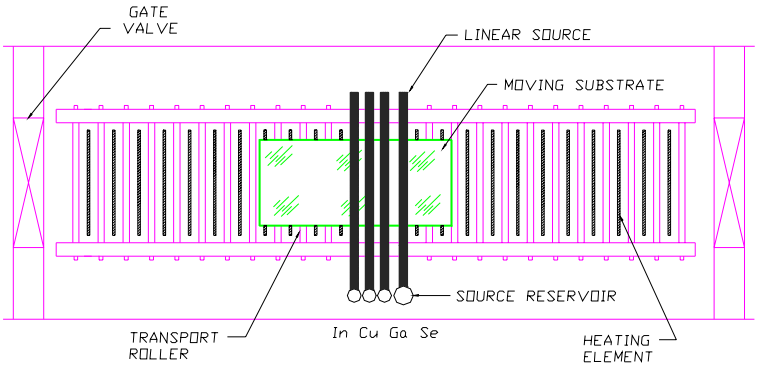

Fig. 3.1. Schematic of various elements of an in-line deposition system for large area CIGS.

Figure 3.2 shows thickness calibration profiles for Cu, In, and Ga evaporations, and a thickness profile of a CIGS film, all measured across the width of the glass substrate i.e. in the direction of the source axes. (These four profiles are not interrelated.) The films were deposited in a scanned mode. The depositions of Cu, In, and Ga were conducted in the presence of Se and onto a heated substrate to prevent condensation of elemental Se. The deposited material is therefore a metal selenide. The source times and temperatures were 10, 5, and 5 minutes, and 1390, 1025, and 1080°C, respectively. Acceptable thickness uniformity is demonstrated for Cu, In, and Ga, and good overall thickness uniformity is demonstrated for CIGS. For CIGS, the thickness is constant to within ±6%. The average film deposition rates immediately under the metal sources were about 60 A/s for Cu, 80 A/s for In, and 30 A/s for Ga. In later work, a cross-plate (parallel to the source axis) standard deviation in thickness of 0.04 μm was achieved for a CIGS film 2.4 μm in thickness.

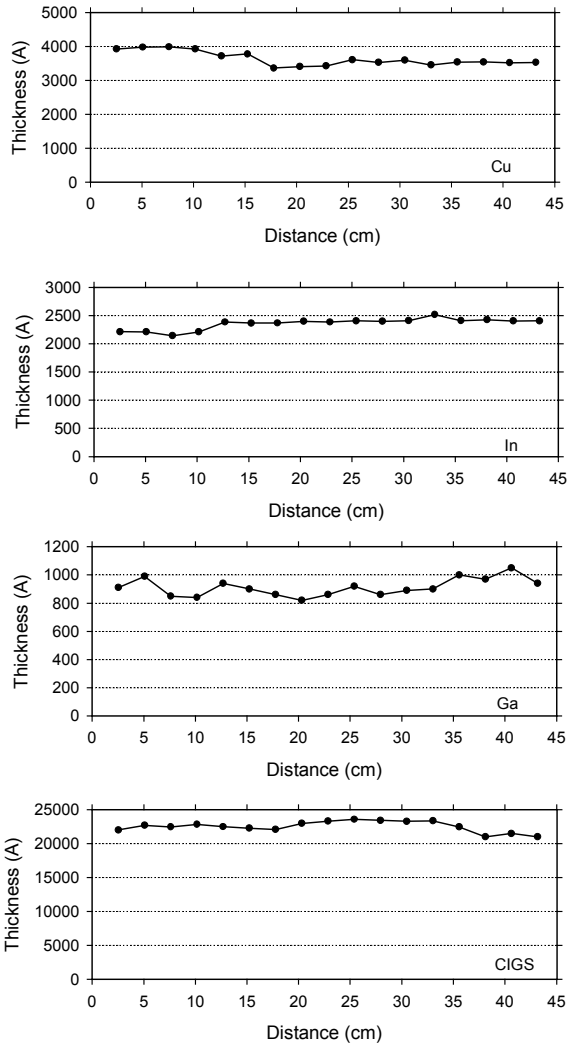

Fig. 3.2 Thickness distributions for Cu, In, Ga, and CIGS along the direction of the linear sources

To further characterize the linear source, depositions were made using Se. Three static depositions were made onto stationary, unheated substrates (one deposition per substrate) at nominal Se source temperatures of 280, 300, and 320°C. To perform the deposition, the Se was brought to a stable temperature, the plate was translated rapidly into position under the linear source and kept there for a certain time, and then the plate was withdrawn. Times under the source were 5, 5, and 2 minutes for the three depositions. These static footprints of the intrinsic deposition profile from the linear source were analyzed using a stylus profilometer in directions parallel and perpendicular to the source axis; two of the profiles are shown in Fig. 3.3. The parallel profile (measured at peak position) is almost flat, but shows a slightly increasing thickness towards one edge of the plate. The reason for this is related to Se supply.

The perpendicular profiles show the expected bell-shaped distribution added to a small background thickness. The peak deposition rates (at the thickest part of the films) were 68, 95, and 116 A/s for the three source temperatures (thicknesses 20400, 28380, and 13880A). The width of the distribution did not depend on source temperature. At first, the expected profile was calculated assuming a line source of constant strength and a cosine law emission from each element of the source. This predicts that, for a source-substrate distance h, the thickness t(x) along the substrate should vary according to

$$t(x) \propto 1/h \,.\, 1/(1 + (x/h)^2)^{3/2} \tag{1}$$

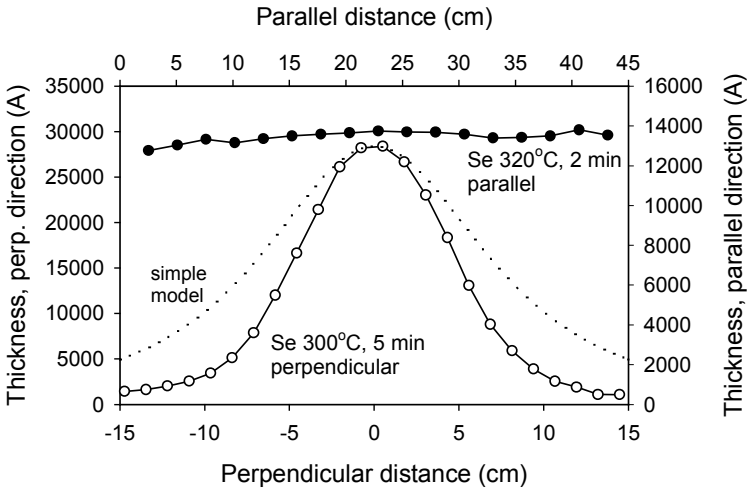

Fig. 3.3. Thickness profiles for static Se depositions

where x is the distance from the line in the substrate lying directly under the source axis. This distribution is plotted as a dotted curve in Fig. 3.3. The width of this distribution is much larger than that exhibited by the film data. In order to reproduce the more peaked thickness distribution found experimentally we repeated the calculation for a $\cos^3(\theta)$ emission law. This predicts that for a source-to-substrate distance h, and a mass emission rate m_e, the film mass m(p) at a distance p along the substrate is

$$m(p) = \tfrac{3}{4}\, m_e\, h^4/(h^2 + p^2)^{5/2} \tag{2}$$

Even better agreement with experiment is found for a $\cos^{3.5}(\theta)$ emission law. This is shown in Figure 3.4, which shows the normalized thickness for a Se film deposited onto a stationary substrate from a linear source (solid data points) and the result of the flux integration (curve) [7].

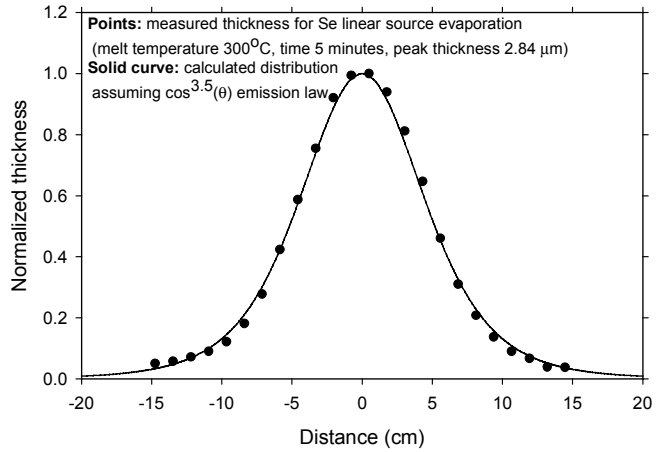

Fig. 3.4. Experimental and modeled thickness profile for linear source evaporation.

4.0 CIGS Analysis

4.1 Resistance

A quick indicator of copper content in a CIGS film is the film's electrical resistance. This was measured for 75 different pilot line CIGS samples using two suitable contacts applied to the top surface of the CIGS/Mo/glass sample. The global composition of each film was also measured by ICP in a region adjacent to that used for the resistance check. In Fig. 4.1 we show a scatter plot of log resistance versus the Cu/(In+Ga) ratio. This reveals a linear relation between log R and Cu ratio for films in the Cu-poor regime (Cu ratio < 1). However, once the film becomes Cu-rich (Cu ratio > 1), the resistance falls abruptly by two to three orders of magnitude, and within the accuracy of the measurement, appears independent of Cu ratio. The sharp fall in resistance signifies the appearance of a highly conductive Cu_2Se phase in the film. This metallic phase leads to shunting of devices and poor cell performance. It is generally reported that the Cu ratio for optimal cell performance lies in the range 0.8 to 0.95. This would imply a film resistance in the range 20kΩ - 200kΩ, which is consistent with our rule of thumb used for several years.

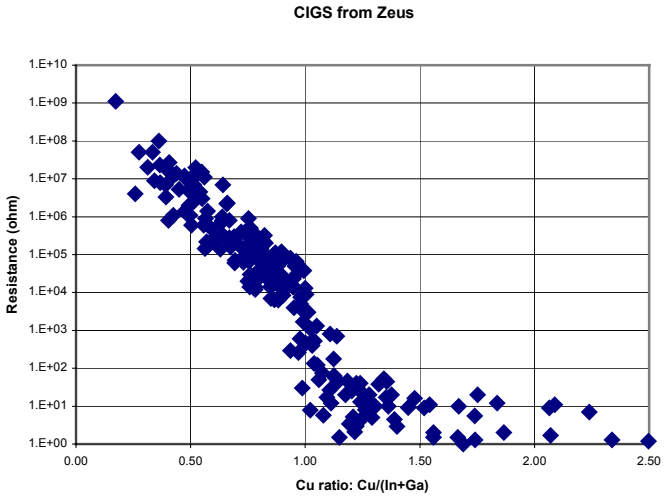

Fig. 4.1. Resistance versus Cu content for CIGS films

4.2 Composition

The ICP-AES machine (inductively-coupled-plasma atomic emission spectrometer) was set up and calibrated using a certified solution containing 100ppm each of Cu, In, Ga, and Se. Extensive tests were conducted to be sure of our results. In particular, linearity tests conducted by diluting the solution revealed the machine to exhibit non-negligible non-linearity. By changing the default operating parameters we were able to greatly reduce this effect. Using a piece of "16%" CIGS donated by NREL, we were able to compare the composition results obtained at EPV and NREL on samples of CIGS cut from the same substrate. The results are summarized in table 4.1 below.

Table 4.1. Composition determination of CIGS run C1297

Measurement location	Cu (%)	Ga (%)	In (%)	Se (%)	Cu/(In+Ga)	Ga/(In+Ga)
EPV	24.3	7.5	18.1	50.1	0.95	0.29
NREL	24.6	8.3	17.9	49.2	0.94	0.32

The reasonably good agreement between the two laboratories gives us confidence that the results are correct.

The ICP machine has been used to quickly home in on the desired composition of CIGS produced in the Zeus large area system. Previously, we had no way of determining the Ga/(In+Ga) ratio in our films. ICP analysis showed that this ratio could drift as high as 0.60 without our fully realizing it. Similarly, the Cu/(In+Ga) ratio could be as low as 0.65 in working devices. Now, reasonable compositions can be achieved in at most 4-5 runs from an arbitrary

starting point. This is illustrated in the appended table 4.2 for runs Z1274 – Z1277, an early exercise in using the ICP to direct Zeus parameter choice.

Table 4.2. An early exercise in composition convergence using ICP

Run #	Cu	Ga	In	Se	Se/(Cu+Ga+In)	Cu/(In+Ga)	Ga/(In+Ga)
Z1274	14.91%	17.62%	12.86%	54.61%	1.20	0.49	0.58
Z1275	14.52%	9.82%	20.63%	55.04%	1.22	0.48	0.32
Z1276	19.22%	7.69%	20.55%	52.54%	1.11	0.68	0.27
Z1277	22.96%	6.01%	19.43%	51.60%	1.07	0.90	0.24

In the early days of having in-house ICP data it appeared that cell efficiencies in the 8 – 12% range were almost always obtained provided that the CIGS composition was approximately correct. Unfortunately, this hypothesis later proved to be incorrect, implying that a reasonable global film composition is not sufficient to ensure good device results.

Another early study using the ICP machine concerned the Se to metal ratio in binary selenides deposited for calibration purposes. The metals were deposited in the presence of Se, the Cu, Ga, and In source temperatures being 1340°C, 1060°C, and 1100°C, respectively. As shown in table 4.3 below, the stoichiometry of the principal metal selenide was found to be InSe, GaSe, and Cu_2Se with a Se source temperature of 260°C (low Se flux), but In_2Se_3 and Ga_2Se_3 with a Se source temperature of 290°C (higher Se flux).

Table 4.3. Dependence of Se/metal ratio on Se source temperature

Sample ID	Thickness (A)	Se source temp (°C)	Cu (%)	Ga (%)	In (%)	Se (%)	Se/metal ratio
1031 indium selenide	7000	260			47	52	1.03
1031 gallium selenide	2600	260		46		51	1.09
1031 copper selenide	4000	260	67			35	0.53
1101 indium selenide	8000	290			42	58	1.36
1101 gallium selenide	2500	290		42		59	1.46

For CIGS films prepared by translating the substrate under the sources, Figure 4.2 shows the composition ratios Cu/(In+Ga) and Ga/(In+Ga), as determined in-house by ICP, as a function of distance along the substrate i.e. in a direction normal to the source axes [7]. Good compositional uniformity is obtained. The figure also maps diagnostic device parameters V_{oc}, FF and efficiency along the plate. It would appear that FF is controlled by a factor that is not directly related to composition.

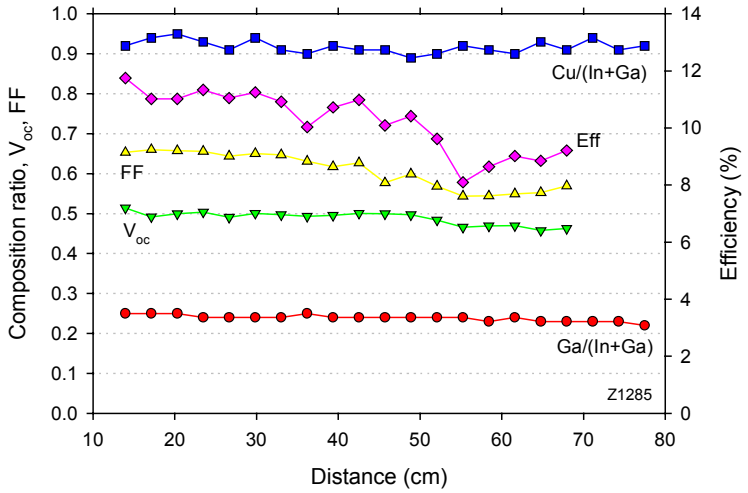

Fig. 4.2. CIGS composition and device parameters as a function of position along the plate.

At present, the composition of every film produced in both the pilot line system (Zeus) and R&D system (Hercules) is determined by ICP. Table 4.4 below shows typical data for a sequence of Hercules runs from H95 to H104. Given that the recipes, and even hardware details, are tweaked for almost every run, it is nevertheless evident that quite reasonable control of global composition can be maintained.

Table 4.4. Composition for a sequence of Hercules CIGS films, as determined by ICP

Run and sample ID #	Cu	Ga	In	Se	Se/Σ	Cu/ (In+Ga)	Ga/ (In+Ga)	R (Ω)
H95-1AI	23.58%	8.79%	17.13%	50.50%	1.02	0.91	0.34	1.0E+04
H95-1BI	24.08%	8.51%	16.62%	50.79%	1.03	0.96	0.34	7.0E+03
H95-6I	21.75%	7.04%	19.32%	51.89%	1.08	0.83	0.27	1.6E+04
H96-1AI	23.13%	8.84%	17.93%	50.10%	1.00	0.86	0.33	2.6E+04
H96-6AI	22.11%	7.61%	19.41%	50.87%	1.04	0.82	0.28	6.0E+04
H96-6BI	21.06%	7.24%	20.23%	51.47%	1.06	0.77	0.26	1.0E+05
H97-1AI	22.05%	8.96%	17.84%	51.15%	1.05	0.82	0.33	5.0E+04
H97-1BI	22.51%	8.76%	17.87%	50.85%	1.03	0.85	0.33	1.1E+05
H97-6AI	20.86%	7.64%	19.74%	51.76%	1.07	0.76	0.28	1.0E+05
H97-6BI	20.77%	7.45%	20.28%	51.50%	1.06	0.75	0.27	3.0E+04
H98-1AI	25.73%	11.05%	13.93%	49.30%	0.97	1.03	0.44	1.1E+03
H98-1BI	24.05%	10.17%	15.69%	50.09%	1.00	0.93	0.39	1.3E+04
H98-6AI	23.26%	8.99%	17.23%	50.52%	1.02	0.89	0.34	2.0E+04
H98-6BI	20.83%	8.24%	19.73%	51.20%	1.05	0.74	0.29	1.7E+05
H99-1AI	21.91%	9.84%	17.00%	51.26%	1.05	0.82	0.37	2.0E+04
H99-1BI	15.63%	10.48%	18.23%	55.66%	1.26	0.54	0.36	2.2E+04
H99-6AI	20.14%	8.21%	19.18%	52.46%	1.10	0.74	0.30	2.7E+05
H99-6BI	20.24%	8.27%	19.24%	52.24%	1.09	0.74	0.30	1.2E+05
H100-1AI	25.34%	9.48%	15.13%	50.04%	1.00	1.03	0.39	9.0E+03
H100-1BI	23.88%	8.89%	16.39%	50.84%	1.03	0.94	0.35	1.5E+04
H100-6AI	23.00%	8.17%	17.90%	50.93%	1.04	0.88	0.31	1.0E+05
H100-6BI	21.48%	7.72%	18.85%	51.95%	1.08	0.81	0.29	1.8E+05
H101-1AI	20.70%	8.17%	19.79%	51.35%	1.06	0.74	0.29	1.6E+05
H101-1BI	21.10%	8.09%	19.58%	51.23%	1.05	0.76	0.29	2.2E+05
H101-6AI	18.97%	6.78%	21.28%	52.97%	1.13	0.68	0.24	3.0E+05
H101-6BI	19.24%	6.90%	21.50%	52.36%	1.10	0.68	0.24	1.7E+05
H102-1AI	19.55%	8.85%	19.35%	52.25%	1.09	0.69	0.31	6.0E+05
H102-1BI	19.56%	8.77%	19.03%	52.64%	1.11	0.70	0.32	5.5E+05
H102-6AI	18.09%	7.45%	21.02%	53.43%	1.15	0.64	0.26	7.3E+05
H102-6BI	18.10%	7.45%	21.00%	53.45%	1.15	0.64	0.26	7.0E+05
H103-1AI	21.34%	8.09%	19.22%	51.35%	1.06	0.78	0.30	5.4E+05
H103-1BI	21.68%	8.12%	19.06%	51.15%	1.05	0.80	0.30	5.0E+05
H103-6AI	19.69%	7.04%	21.13%	52.14%	1.09	0.70	0.25	8.7E+05
H103-6BI	20.05%	7.01%	21.05%	51.90%	1.08	0.71	0.25	6.0E+05
H104-1AI	19.96%	8.29%	19.87%	51.88%	1.08	0.71	0.29	4.5E+05
H104-1BI	19.93%	8.27%	19.58%	52.22%	1.09	0.72	0.30	5.2E+05
H104-6AI	18.42%	7.10%	21.92%	52.56%	1.11	0.63	0.24	5.0E+05
H104-6BI	18.49%	6.98%	21.69%	52.84%	1.12	0.65	0.24	2.2E+05

4.3 Morphology

Once correct film composition has been achieved, the morphology of the films becomes of increasing interest. This is studied in-house using a JEOL JSM-5410 scanning electron microscope. A large variety of surface features have been observed, and the correlation with device performance has not yet been attempted, save to observe that the presence of a high density of deep voids does not bode well for high efficiency. By detaching portions of the film from the substrate the opportunity is gained to observe cross-sections and even the rear surface of the CIGS layer. In Fig. 4.3 we show a cross-section of film H87, which yielded a 9.3% device. A compact grain structure is evident.

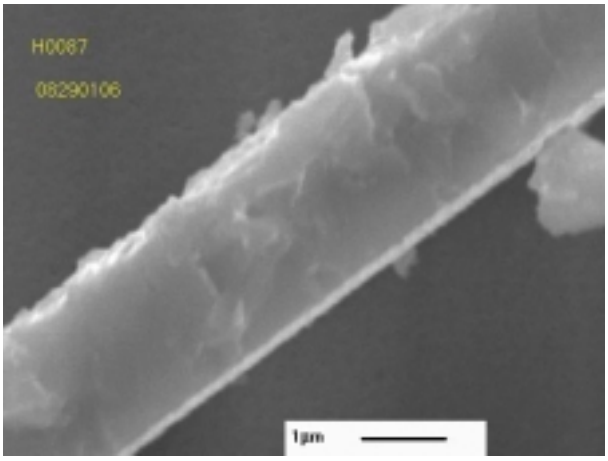

Fig. 4.3. Scanning electron micrograph of CIGS film cross-section

In Fig. 4.4 we show an SEM micrograph of the rear surface of a detached portion of film Z1284. The layer exhibits a fine-grained material. The voids appear to be a common feature of the Mo-CIGS interface, but their origin and significance are at present unknown.

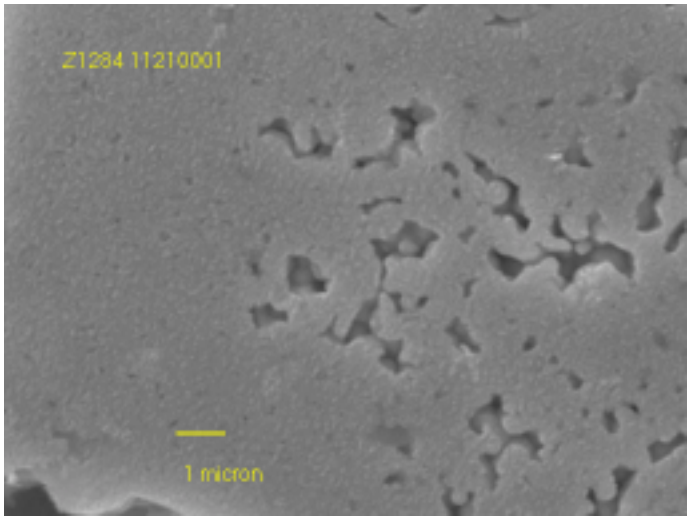

Fig. 4.4. Scanning electron micrograph of the rear surface of a portion of a CIGS film detached from the Mo

4.4 Depth Profiles

In some of the earlier Hercules device recipes, the Cu and Ga of the first stage were loaded into the same boat and were evaporated from that boat. Similarly, in the third stage the Cu and Ga were loaded into a single boat. It has been reported that the elements Cu and Ga alloy and are evaporated simultaneously, but in the case of the third stage (where Cu mass greatly exceeds Ga mass) it is not evident whether all of the Ga is evaporated prior to the completion of Cu evaporation, or whether Ga is present at the end of the evaporation. To test this, 1.14g Cu and 0.21g Ga were loaded intermixed into the same boat and were evaporated (run H62) onto an unheated Mo/glass substrate to limit inter-diffusion. A sample was sent for depth profiling, and the results are shown below in Fig. 4.5. Although the Ga peaks closer to the Mo interface than does the Cu, it certainly appears that Ga is present with Cu near the outer surface of the film. Based on this result, this particular third stage should be capable of supplying Ga to the outermost layers of the growing CIGS, i.e. in the junction region.

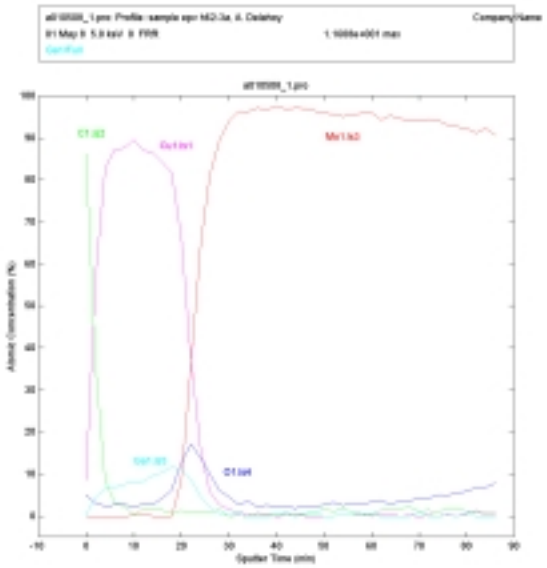

Fig. 4.5. Auger profile of a film resulting from Cu-Ga evaporation

A similar recipe was tried in the pilot line system. Because most of the Ga was deposited early on, an obvious question concerns the distribution of Ga throughout the depth of the CIGS film. To this end, a piece of Z1232 that had undergone R&D CdS dipping, but had not been further processed, was cut out and sent to NREL for Auger depth profiling. The profiles are shown in Fig. 4.6 below. In contrast to the relatively flat Ga profile exhibited by EPV's standard pilot line CIGS (as shown in the Phase II Annual report), this material exhibits what is believed to be a more desirable profile, with the Ga concentration increasing from a relatively low value near the surface to a substantially higher value at the back of the film. (In contrast, the Cu distribution is always homogeneous, implying a high mobility for Cu atoms.) This Ga profile should result in a back-surface field that increases collection of pairs created by deeply-absorbed long-wavelength photons, thereby increasing J_{sc}. Another view is that V_{oc} is enhanced by reduction of back surface recombination. Note that the ratio of Ga/(In+Ga) is also shown in the figure. We suspect that a lower ratio at the surface (about 0.22) would result in higher quality material; the ratio at the back is probably satisfactory. The PV parameters of a device made on this material were V_{oc} 539 mV, J_{sc} 31.4 mA/cm^2, FF 67.0%, and efficiency 11.3%. It may also be significant that sulfur from the CdS appears to penetrate more deeply than the Cd.

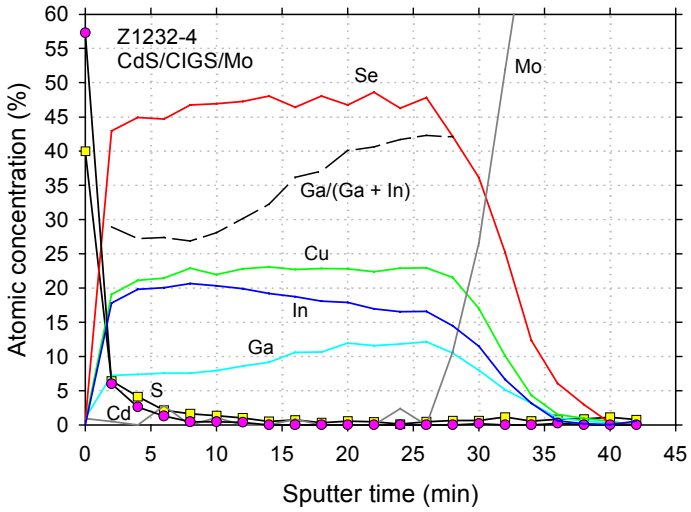

Fig. 4.6. Auger depth profile for pilot line CIGS produced by linear source evaporation.

The important role of substrate temperature in determining the Ga profile is illustrated by the SIMS depth profile of runs H89 and H93 (Figs. 4.7 and 4.8). In run H89 the evaporation stages were Cu+Ga/Ga/In, and a final stage temperature of 540°C was used. A roughly flat Ga profile was achieved, despite there being no Ga in the third stage. In run H93 the evaporation stages were identical, except that the temperature never exceeded 480°C. In this case the Ga concentration falls from its value in the rear half of the film to about 1% of this value near the top of the film. The enormously different QE spectra, reflecting the difference in the minimum energy gap of the two CIGS layers, are shown in section 5.1 below.

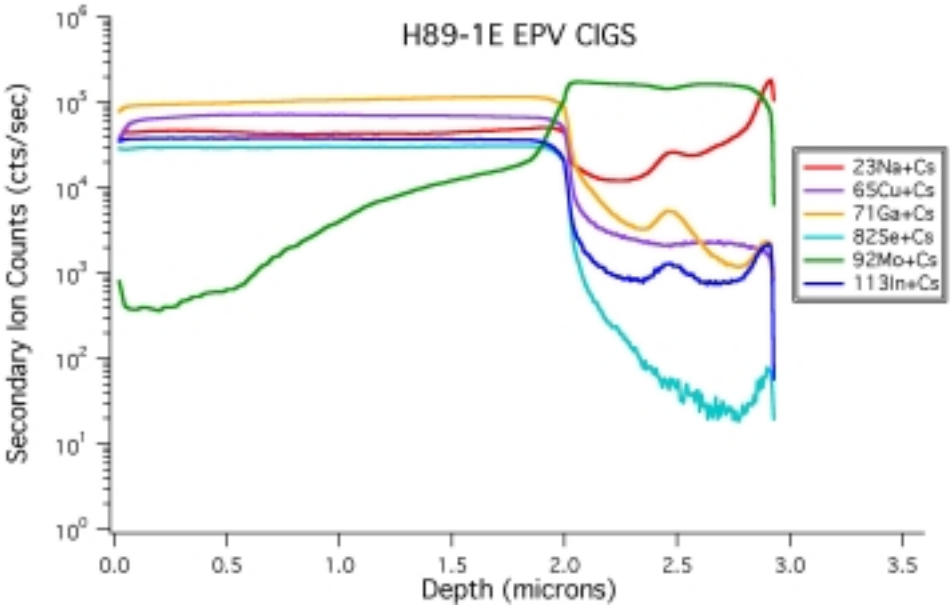

Fig. 4.7. SIMS Profile of H89

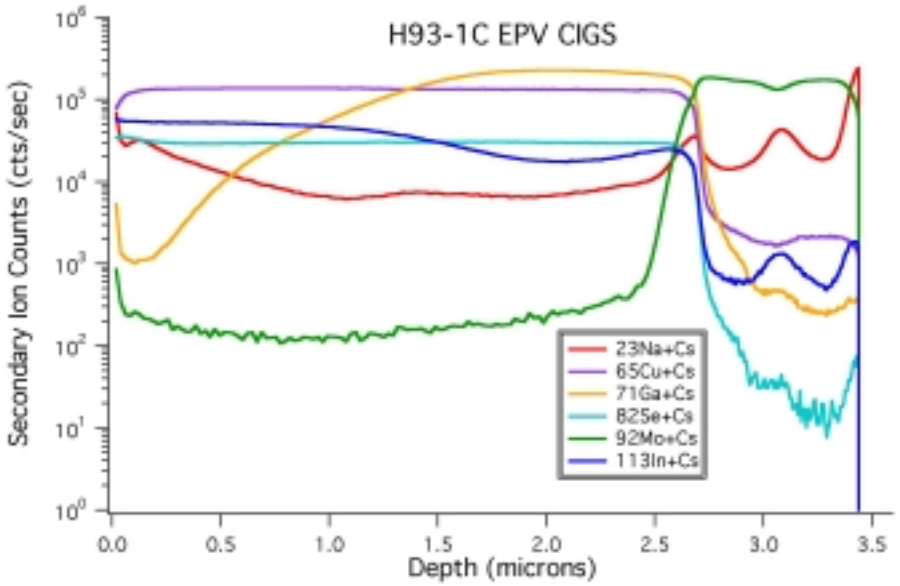

Fig. 4.8. SIMS profile of H93

4.5 Non-Contact measurements

A non-contact measurement has been devised that appears to show significant correlation with Cu/(In+Ga) ratio as measured by ICP. Thus, Fig. 4.9 shows the copper ratio versus the parameter derived from the measurement for samples ranging in Cu ratio from 0.3 to 1.4.

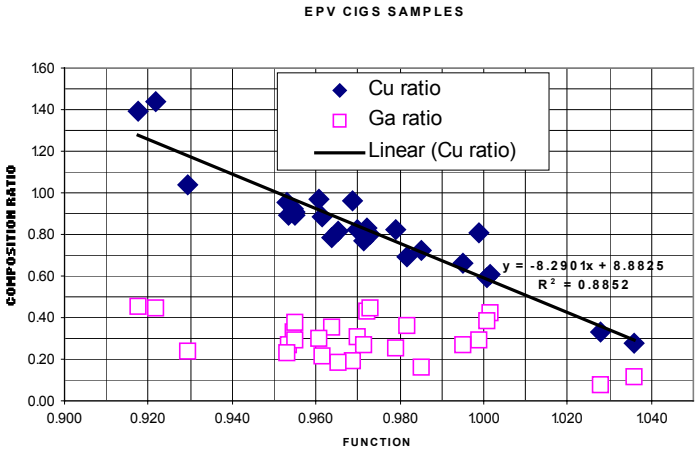

Fig. 4.9. Correlation of a parameter determined from non-contact measurements with Cu/(In+Ga) ratio

5.0 Device results

5.1 Standard devices with CdS

In the pilot line system, diagnostic devices have been prepared on portions of the substrate with efficiencies of up to 12% using CBD CdS (V_{oc} = 581 mV, J_{sc} = 30.1 mA/cm^2, FF = 68.7%). Limited work with Cd-containing partial electrolytes produced highly variable results, although a maximum V_{oc} of 500 mV was achieved.

CIGS was also produced in the R&D scale Hercules system. Using CBD CdS, a best cell efficiency of 13.3% was achieved (V_{oc} = 569 mV, J_{sc} = 34.1 mA/cm^2, FF = 68.1%). This cell possessed a CGS underlayer. By varying the minimum Ga content in the bulk of the cell, the long-wavelength QE edge could be varied from 1000 nm to 1300 nm (Fig. 5.1). It is notable that the efficiencies of two of the devices shown in this figure were almost identical (H89 8.3% and H93 8.1%) despite the very different band edges. To a large extent, V_{oc} was traded for J_{sc} (535mV and 26.6mA/cm^2 versus 414mV and 35.4mA/cm^2). The Ga profiles causing the shift of the band edge for these particular devices were discussed in section 4.4 above; the CIGS composition is given in Table 5.1 below. The I-V curve for the third device shown in Fig. 5.1 (H101) is shown in Figure 5.2. This device exhibited a fill factor of 67.9%. Material from the Hercules system was used to support cell fabrication for the novel buffer layer program (see section 5.3).

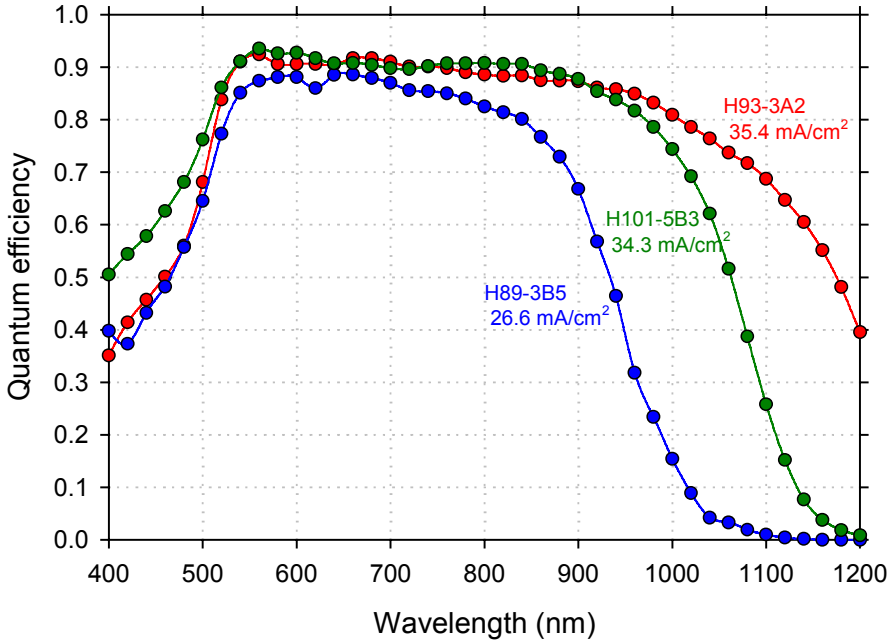

Fig. 5.1. Quantum efficiency of devices made with Hercules CIGS of various band gaps.

Table 5.1. Film composition obtained by ICP

Sample	Cu (%)	In (%)	Ga (%)	Se (%)	Cu/(In+Ga)	Ga/(In+Ga)
Z1301	21.4	14.7	12.0	51.9	0.80	0.45
H89	15.5	22.1	8.9	53.6	0.50	0.29
H93	22.9	17.9	8.5	50.7	0.87	0.32

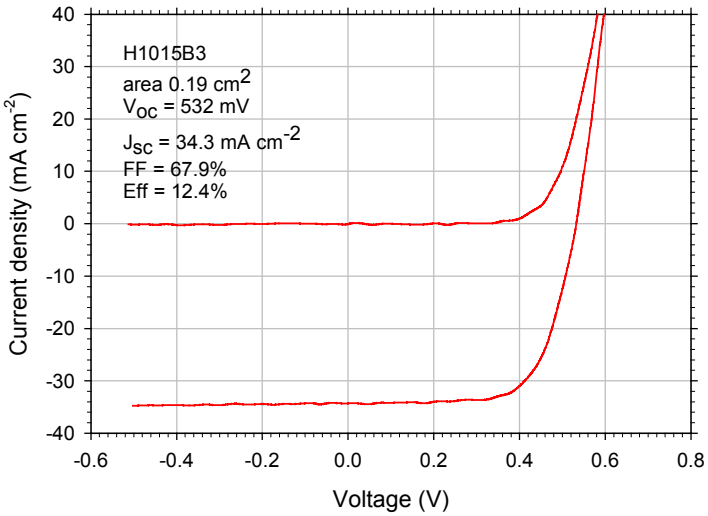

Fig. 5.2. I-V curve for a 12.4% device with CBD CdS

While it might be expected that Ga/(In+Ga) controls bandgap and hence J_{sc}, a relationship such as J_{sc} decreases with increasing Ga/(In+Ga) cannot be universally true, since it is contradicted by the data for H89 and H93 discussed in detail above. (It will be recalled that the J_{sc}s were 26.6mA/cm^2 and 35.4mA/cm^2, the Ga ratios 0.29 and 0.32, but that the Ga profiles were radically different.) Nevertheless, as can be seen from Fig. 5.3, a general trend may be said to exist between J_{sc} and Ga/(In+Ga).

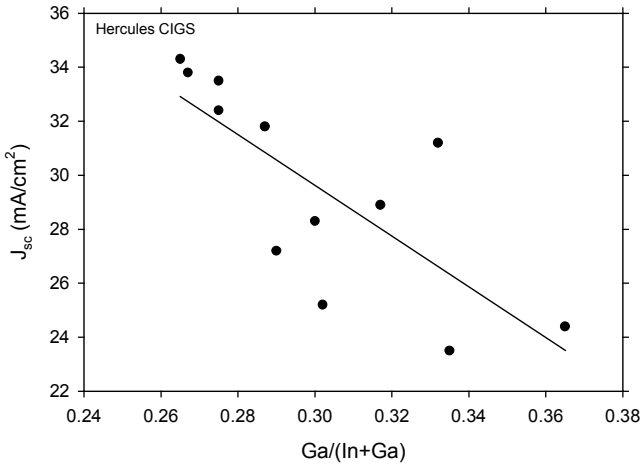

Fig. 5.3. Dependence of J_{sc} on Ga/(In+Ga) for Hercules films

5.2. High V_{oc} Devices with CdS

Linear source evaporation has also been used to produce high Ga content material over large areas. Figure 5.4 shows the I-V curve of an 11.2% diagnostic device with V_{oc} = 596 mV, J_{sc} = 27.9 mA/cm^2, FF = 67.7% prepared in run Z1301. The latter devices exhibited Cu/(In+Ga) = 0.80 and Ga/(In+Ga) = 0.45 as measured by ICP (Table 5.1 above), and had a long-wavelength QE edge at 1020nm. High voltage, lower current devices such as these are particularly suitable for modules.

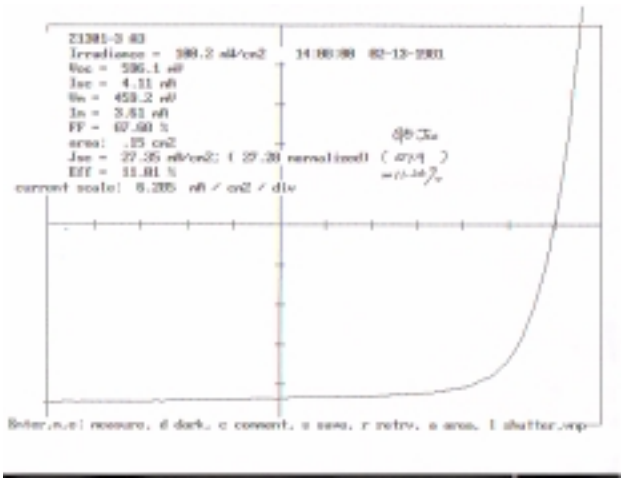

Fig. 5.4. I-V curve for 11.2% cell prepared using pilot line CIGS with Ga/(In+Ga) = 0.45.

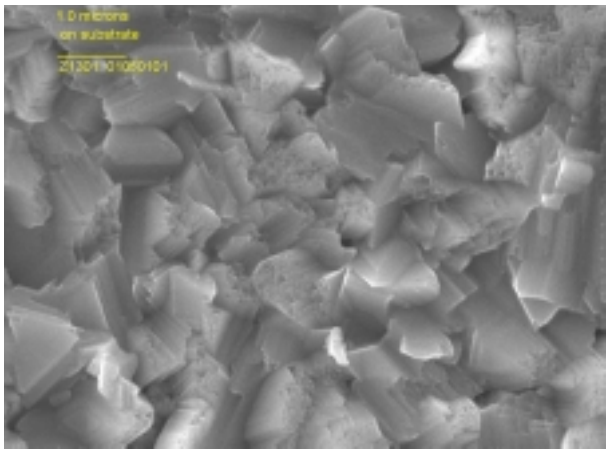

Fig. 5.5. Scanning electron micrograph of CIGS film with high Ga content (Z1301)

5.3 Devices with ZIS

The highest efficiency CIGS cells are conventionally fabricated using a CdS buffer layer prepared by chemical bath deposition. This process is not manufacturing-friendly because of the liquid waste and the use of cadmium. In an attempt to solve these problems, EPV has investigated ternary compounds that can be directly deposited by vacuum evaporation as potential buffer layer materials [4,9]. Since Zn is an n-type dopant in CIS, and since In and Se are already present in CIS or CIGS, we contemplated the use of $ZnIn_xSe_y$ (ZIS) as a buffer material. Previous work explored co-evaporation of Zn, In, and Se onto CIGS [8].

ZIS films were deposited by evaporation of ZIS granules from an open tungsten boat. At sufficiently high substrate temperatures the defect chalcopyrite $ZnIn_2Se_4$ was obtained. From a plot of $(\alpha h\nu)^2 \sim (h\nu - E_g)$ a bandgap E_g of 1.9–2.0 eV was deduced. The temperature dependence of the dark and photoconductivity of a 0.53μm film deposited at 270°C is shown in Fig. 5.6. Writing $\sigma_d = \sigma_0 \exp(-\Delta E/kT)$, an activation energy ΔE of 0.28eV is obtained above room temperature. At 1 sun the photoconductivity was $\sigma_{ph}=4.9 \times 10^{-4}$ $(\Omega\ cm)^{-1}$.

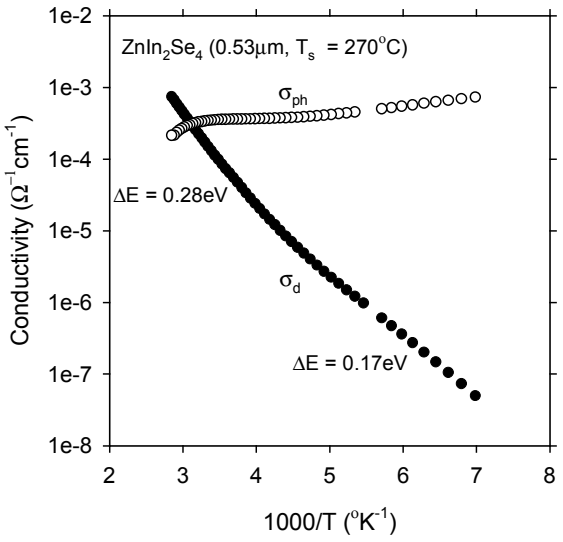

Fig. 5.6. Temperature dependence of the dark conductivity and photoconductivity of a 0.53µm ZIS film.

Another possible ternary buffer material is $ZnGa_xSe_y$ (ZGS). Within the ZIS and ZGS family of materials, EPV has explored several material compositions, with variable results. ZIS itself, however, consistently provides reasonable cell efficiencies [5]. Furthermore, no light soaking effects are seen, unlike the strong increase in V_{oc} exhibited by ZnO/CIGS devices where the ZnO is prepared by the *ROMEAO* process [10].

We have used ZIS as a buffer layer in the configuration ZnO/ZIS/CIGS/Mo/glass, and studied the dependence of cell performance on the substrate temperature T_s during ZIS deposition. In this study, samples were processed with various buffer layers using NREL CIGS from run C1292. The ZIS was evaporated from a baffled source, and the ZnO was sputtered onto all samples simultaneously. Table 5.2 summarizes the results.

Table 5.2. Cell parameters as a function of ZIS buffer deposition temperature.

Contact/ buffer layers	**T_s ZIS** °C	**V_{oc}** mV	**J_{sc}** mA/ cm^2	**FF** %	**Eff.** %	**Comment**
ZnO/ZIS	100	452	15.8	43.8	3.13	
ZnO/ZIS	200	562	30.8	67.2	11.64	
ZnO/ZIS	315	453	22.3	65.3	6.59	
ZnO/ZIS	370	44	4.2	28.2	0.05	
ZnO/CdS	-	610	35.8	74.8	16.33	control

At a T_s of 200°C for the ZIS, an 11.6% cell was achieved with V_{oc} 562 mV, J_{sc} 30.8 mA cm^{-2}, and FF 67.2% (see Fig. 5.7). The cell exhibited no dark-light crossover of the I-V curves. Crossover was observed for higher T_s, and with other ternary buffer compositions. Cell efficiencies using EPV CIGS tended to range from 6% to 9% with voltages up to 500mV.

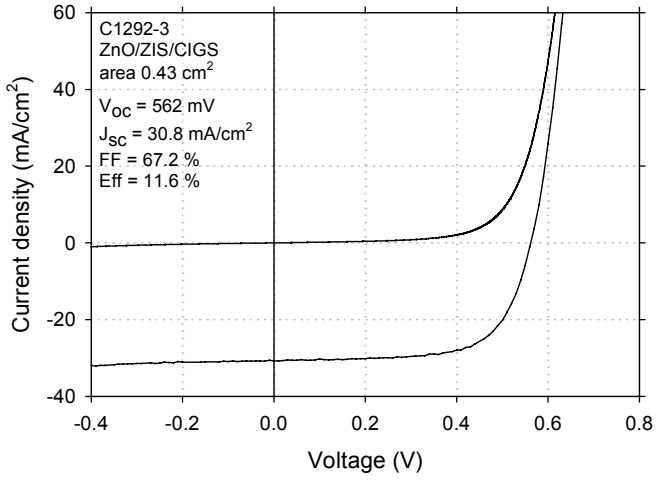

Fig. 5.7. I-V curve for an 11.6% CIGS cell with vacuum-deposited, non-Cd, ternary buffer layer (ZIS).

Many early ZIS/CIGS devices exhibited a QE curve that never exceeded a QE of 0.7 at any wavelength. Two effects were discovered that contributed to this apparent optical absorption. One effect was related to darkening of the ZnO. This was corrected through proper deposition procedures. The second effect appears to be due to sub-gap optical absorption in the ZIS film. The magnitude of this effect seems to be variable, and its dependence on deposition conditions is being studied. Over 4mA/cm^2 was gained through minimization of these effects, as shown in Fig. 5.8.

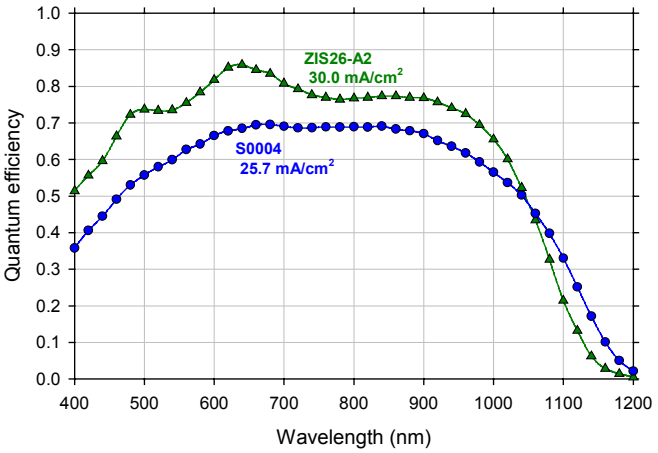

Fig. 5.8. Quantum efficiency of early and improved CIGS devices with ZIS buffer layers

The evaporation behavior of $ZnIn_2Se_4$ was investigated by monitoring the film deposition rate as a function of source temperature during the complete evaporation of a fresh charge of $ZnIn_2Se_4$. A small emission peak was discovered at a source temperature of about 290°C, followed by the principal emission peak at about 850-860°C, with no other peaks at higher temperatures (see Figure 5.9). Analysis of material (in-house by EDS) captured on a glass slide during the initial emission revealed it to be selenium.

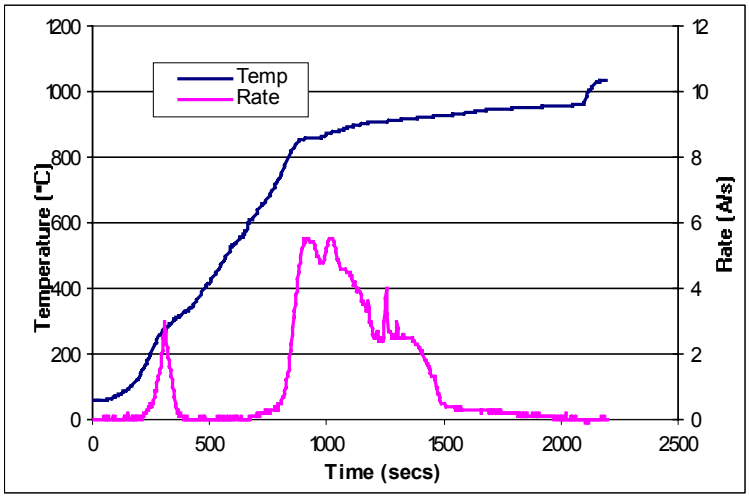

Fig. 5.9. ZIS deposition rate as a function of evaporation time and source temperature.

5.4 a-Si/CIGS Tandem Devices

As a manufacturer of same-bandgap, a-Si/a-Si thin film modules (the EPV-40, 40W, 0.79m^2 module) and *Integrated Manufacturing Systems*, EPV is interested in the lamination of monolithic a-Si plates to CIGS plates to form a-Si/CIGS tandem modules. We calculate that, in this way, a 8% CIGS module can be turned into a 10.4% a-Si/CIGS module.

Previous attempts to develop this technology were stymied by large parasitic absorption of light intended for the CIGS plate. We have started a program to understand and solve this problem. If a filter consisting of soda-lime glass/SnO_2:F/a-Si/ZnO:Al is simply placed in front of a bare CIGS device with J_{sc} of 34.8 mA/cm^2, the J_{sc} of the CIGS device is massively reduced to 5.6 mA/cm^2. By various means, we have reduced the losses so that a J_{sc} of 12.9 mA/cm^2 is obtained (Fig. 5.10).

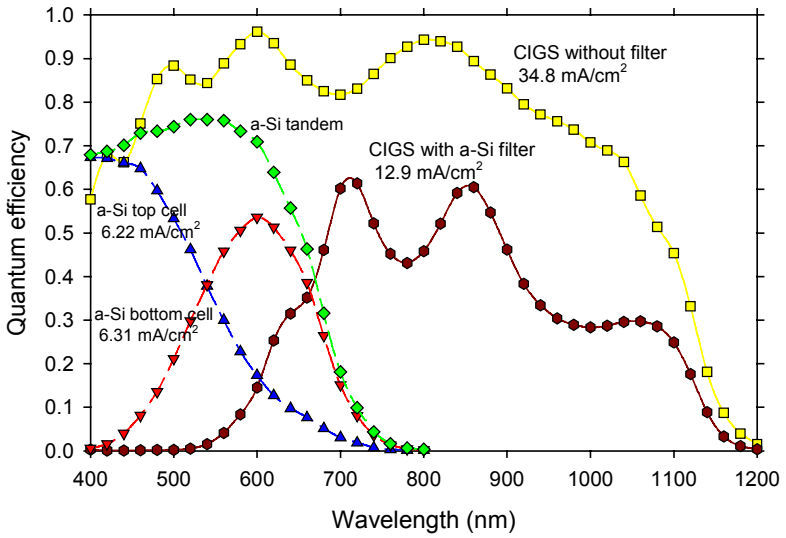

Fig. 5.10. Quantum efficiency of filtered and un-filtered CIGS devices, with QE of tandem a-Si for comparison.

6.0 Zinc oxide

One method of preparing large area doped zinc oxide (for use as a transparent contact in CIGS modules) is DC sputtering from a $ZnO:Al_2O_3$ target. We have previously reported properties obtainable by sputtering from a 56 cm target onto unheated substrates [11]. Here we report a very useful improvement in both conductivity and transmission by deposition onto heated substrates. Figure 6.1 below shows an improvement in conductivity from 420 to 870 $\Omega^{-1}cm^{-1}$ and weighted transmission from 88.3 to 92.2% upon increasing the deposition temperature to 190°C. The increased ZnO conductivity allows a sheet resistance of 20 Ω/sq. to be achieved at a thickness of less than 0.6 μm.

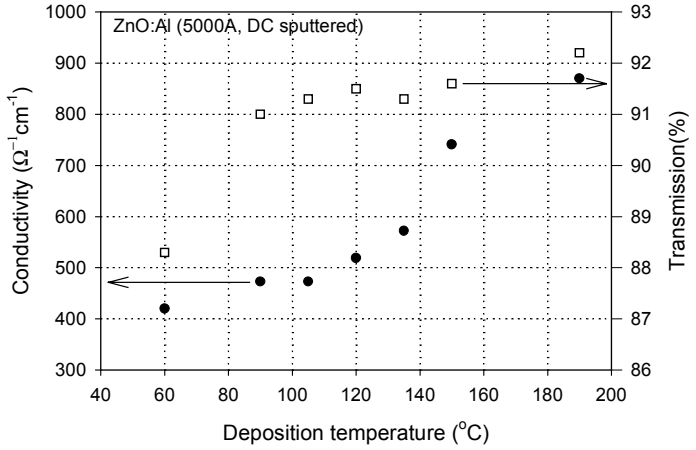

Fig. 6.1. Conductivity and transmission of sputtered ZnO:Al versus deposition temperature.

7.0 Modules

Full size (4300 cm^2) modules were fabricated with 81 monolithically-integrated segments, and exhibited open-circuit voltages up to 36.9 V. With an average cell voltage of 456 mV, the standard deviation in cell voltage across the plate was typically 45 mV. The best combination of CIGS module efficiency and module size was obtained at 3100 cm^2 with an efficiency of 7.6%. The Mo electrode was patterned by laser scribing, while the second and third patterning steps were performed by mechanical scribing. Parameters down the plate, i.e. in the direction of plate translation, tended to be more uniform than across the plate. For example, for one particular plate, the following mean values and standard deviations (SD) were obtained for measurements made at 21 positions spread over 70 cm down the plate: Cu/(In+Ga) 0.92 (SD 0.016), Ga/(In+Ga) 0.24 (SD 0.008), V_{oc} 488 mV (SD 16 mV), Eff 10.2% (SD 1%).

EPV, Inc.
Thin-Film CIGS Photovoltaic Technology
Subcontract No. ZAK-8-17619-21

Phase III Summary

- State-of-the-art capabilities were demonstrated for Mo, CIGS, and ZnO depositions at coating widths of 45 cm.
- The CIGS is formed by linear source evaporation onto moving substrates using multiple line sources.
- The linear sources were characterized according to deposition uniformity and angular dependence of emitted flux.
- Uniformity maps were generated for CIGS composition and device performance over large areas.
- Large area CIGS modules were produced with V_{oc}'s up to 36.9 V.
- High Ga content CIGS devices were produced in the pilot line system with an efficiency of 11.2% (596 mV, 27.4 mA/cm^2, FF 67.7%)
- The minimum bandgap in R&D CIGS was successfully controlled through Ga content and Ga profile. A reliable recipe was developed that yielded a best efficiency of 12.4% (532 mV, 34.3 mA/cm^2, FF 67.9%).
- A promising source material ($ZnIn_2Se_4$) was synthesized and used for buffer layer deposition, resulting in an 11.6% cell on NREL CIGS (562 mV, 30.8 mA/cm^2, FF 67.2%).
- Deposition rate from a charge of ZIS was recorded as a function of evaporation time and source temperature.
- Current generated in the CIGS component of an a-Si/a-Si/CIGS stacked device was increased from 5.6 to 12.9 mA/cm^2.
- Useful gains in conductivity and transmission of large-area sputtered ZnO:Al were obtained through use of substrate heating.
- EPV is constructing an entirely new CIGS pilot line for scale up and limited manufacturing purposes. The coating width is 65 cm.
- The company's analytical capabilities have been upgraded with the installation of ICP, SEM/EDS, computerized QE, and stylus profilometer facilities.

ACKNOWLEDGMENTS

EPV wishes to thank the following members of EPV's technical staff and support team who contributed to this work: M. Akhtar, J. Cambridge, L. Chen, D. Chorobski, A. Delahoy (Principal Investigator), A. Foustotchenko, B. Fraczkowska, R. Govindarajan, S. Guo, A.S. John, Z. Kiss, R. Lyndall, A. Pogorzelski, A. Ruppert, R. Saramak, F. Sheppard, K. Szewczyk, T. Varvar, J. Wisniewski, F. Ziobro.

The following individuals (and institutions) are also acknowledged for their analyses, experiments, advice, or interest: S. Asher, M. Contreras, R. Noufi, H. Ullal, K. Zweibel (National Renewable Energy Laboratory), J. Sites (Colorado State University), A. Rockett (University of Illinois), R. Birkmire, W. Shafarman (Institute of Energy Conversion/University of Delaware), L. Olsen (Washington State University).

Thanks are due also to all members of the National CIS Team for their collaborations and discussions.

Finally, EPV thanks the US DOE for support under subcontract ZAK-8-17619-21 with NREL.

REFERENCES

[1] A.E. Delahoy and ZJ. Kiss "Photovoltaics – heading towards thin films" Photovoltaics Bulletin (Elsevier Advanced Technology, Oxford, ISSN 1473-8325) Nov. 2001, pp. 8-12.
[2] M.A. Contreras, B. Egas, K. Ramanathan, J. Hiltner, A. Swartzlander, F. Hassoon, and R. Noufi, *Prog. Photovolt: Res. Appl.* **7**, 311-316 (1999).
[3] A.E. Delahoy, J.S. Britt, A.M. Gabor, and Z.J. Kiss, *AIP Conf. Proc. Vol.* ***353*** (AIP, NY, 1996) pp. 3-11.
[4] A.E. Delahoy, J. Bruns, A. Ruppert, M. Akhtar, L. Chen, and Z.J. Kiss "Thin Film CIGS Photovoltaic Technology," Phase II Annual Report, NREL/SR-520-28786 (2000).
[5] A.E. Delahoy, D. Chorobski, F. Ziobro, Z.J. Kiss, *AIP Conf. Proc. Vol.* ***462*** (AIP, NY, 1999) 144-151.
[6] A. Delahoy, J. Bruns, L. Chen, M. Akhtar, Z. Kiss "Advances in Large Area CIGS Technology," *Proc. 28th IEEE PV Specialists Conference*, September 15-22, 2000, Anchorage, AK, pp. 1437-1440.
[7] Delahoy, A.E., Akhtar, M., Cambridge, J., Chen, L., Chorobski, D., Govindarajan, R., Guo, S., Kiss, Z., Ruppert, A., Anna Selvan, J.A., Ziobro, F., "Aspects of Large Area CIGS Technology," *Proc. NCPV Program Review Meeting*, Lakewood, CO, October 14-17, 2001 (NREL/EL-520-31065).
[8] M. Konagai, Y. Ohtake, and T. Okamoto, *MRS Symp. Proc. Vol.* ***426*** (1996) 153-163.
[9] A. Delahoy, M. Akhtar, J. Bruns, A. Ruppert, L. Chen, Z. Kiss. "Ternary Source Materials for CIGS Buffer Layers," *Proc. 16th European PVSEC*, 1-5 May 2000, Glasgow, UK, pp. 767-770.
[10] A.E. Delahoy, A.F. Ruppert, and M. Contreras, *Thin Solid Films* **361-362** (2000) 140-144.
[11] A.E. Delahoy and M. Cherny, *MRS Symp. Proc, Vol.* ***426*** (1996) p. 467.

REPORT DOCUMENTATION PAGE

Form Approved
OMB NO. 0704-0188

1. AGENCY USE ONLY (Leave blank)	2. REPORT DATE	3. REPORT TYPE AND DATES COVERED
	March 2002	Final Technical Report, 16 April 1998 – 15 October 2001

4. TITLE AND SUBTITLE
Thin Film CIGS Photovoltaic Technology:
Final Technical Report, 16 April 1998 – 15 October 2001

5. FUNDING NUMBERS
CF: ZAK-8-17619-21
PVP25001

6. AUTHOR(S)
A.E. Delahoy, J. Cambridge, L. Chen, and Z.J. Kiss

7. PERFORMING ORGANIZATION NAME(S) AND ADDRESS(ES)
Energy Photovoltaics, Inc. (EPV)
P.O. Box 7456
Princeton, NJ 08543 USA

8. PERFORMING ORGANIZATION REPORT NUMBER

9. SPONSORING/MONITORING AGENCY NAME(S) AND ADDRESS(ES)
National Renewable Energy Laboratory
1617 Cole Blvd.
Golden, CO 80401-3393

10. SPONSORING/MONITORING AGENCY REPORT NUMBER
NREL/SR-520-31739

11. SUPPLEMENTARY NOTES
NREL Technical Monitor: Harin S. Ullal

12a. DISTRIBUTION/AVAILABILITY STATEMENT
National Technical Information Service
U.S. Department of Commerce
5285 Port Royal Road
Springfield, VA 22161

12b. DISTRIBUTION CODE

13. ABSTRACT *(Maximum 200 words):* This report describes the state-of-the-art capabilities that were demonstrated for Mo, CIGS, and ZnO depositions at coating widths of 45 cm. The CIGS is formed by linear-source evaporation onto moving substrates using multiple line sources. The linear sources were characterized according to deposition uniformity and angular dependence of emitted flux. Uniformity maps were generated for CIGS composition and device performance over large areas. Large-area CIGS modules were produced with V_{oc}'s up to 36.9 V. High-Ga-content CIGS devices were produced in the pilot-line system with an efficiency of 11.2% (V_{oc} 596 mV, J_{sc} 27.4 mA/cm^2, FF 67.7%). The minimum bandgap in R&D CIGS was successfully controlled through Ga content and Ga profile. A reliable recipe was developed that yielded a best efficiency of 12.4% (V_{oc} 532 mV, J_{sc} 34.3 mA/cm^2, FF 67.9%). A promising source material ($ZnIn_2Se_4$) was synthesized and used for buffer layer deposition, resulting in an 11.6% cell on NREL CIGS (V_{oc} 562 mV, J_{sc} 30.8 mA/cm^2, FF 67.2%). Deposition rate from a charge of ZIS was recorded as a function of evaporation time and source temperature. Current generated in the CIGS component of an a-Si/a-Si/CIGS stacked device was increased from 5.6 to 12.9 mA/cm^2. Useful gains in conductivity and transmission of large-area sputtered ZnO:Al were obtained through use of substrate heating. EPV is constructing an entirely new CIGS pilot line for scale up and limited manufacturing purposes. The coating width is 65 cm. The company's analytical capabilities have been upgraded with the installation of ICP, SEM/EDS, computerized QE, and stylus profilometer facilities.

14. SUBJECT TERMS: PV; CIGS; linear source evaporation; large glass substrate; vacuum deposition; atmospheric pressure selenization; rapid thermal processing; electrodeposition; module encapsulation; tandem junction; a-Si module; Mo back electrode; buffer layer deposition; monolithically-integrated segments; doped zinc oxide

15. NUMBER OF PAGES

16. PRICE CODE

17. SECURITY CLASSIFICATION OF REPORT	18. SECURITY CLASSIFICATION OF THIS PAGE	19. SECURITY CLASSIFICATION OF ABSTRACT	20. LIMITATION OF ABSTRACT
Unclassified	Unclassified	Unclassified	UL